

Quasi-energies, parametric resonances, and stability limits in ac-driven \mathcal{PT} -symmetric systems

Jennie D'Ambroise,¹ Boris A. Malomed,² and P.G. Kevrekidis³

¹*Department of Mathematics, Amherst College, Amherst, MA 01002-5000, USA*

²*Department of Physical Electronics, School of Electrical Engineering,
Faculty of Engineering, Tel Aviv University, Tel Aviv 69978, Israel*

³*Department of Mathematics and Statistics, University of Massachusetts, Amherst, MA 01003-9305, USA*

We introduce a simple model for implementing the concepts of quasi-energy and parametric resonances (PRs) in systems with the \mathcal{PT} symmetry, i.e., a pair of coupled and mutually balanced gain and loss elements. The parametric (ac) forcing is applied through periodic modulation of the coefficient accounting for the coupling of the two degrees of freedom. The system may be realized in optics as a dual-core waveguide with the gain and loss applied to different cores, and the thickness of the gap between them subject to a periodic modulation. The onset and development of the parametric instability for a small forcing amplitude (V_1) is studied in an analytical form. The full dynamical chart of the system is generated by systematic simulations. At sufficiently large values of the forcing frequency, ω , tongues of the parametric instability originate, with the increase of V_1 , as predicted by the analysis. However, the tongues following further increase of V_1 feature a pattern drastically different from that in usual (non- \mathcal{PT}) parametrically driven systems: instead of bending down to larger values of the dc coupling constant, V_0 , they maintain a direction parallel to the V_1 axis. The system of the parallel tongues gets dense with the decrease of ω , merging into a complex small-scale structure of alternating regions of stability and instability. The cubic nonlinearity, if added to the system, alters the picture, destabilizing many originally robust dynamical regimes, and stabilizing some which were unstable.

PACS numbers: 11.30.Er; 72.10.Fk; 42.79.Gn; 11.80.Gw

Recently, a great deal of interest has been drawn to systems featuring the \mathcal{PT} (parity-time) symmetry. Originally, they were introduced as quantum systems with spatially separated and symmetrically placed linear gain and loss. A fundamental property of non-Hermitian \mathcal{PT} -symmetric Hamiltonians is the fact that their spectra remain purely real, like in the case of the usual Hermitian Hamiltonians, provided that the strength of the non-Hermitian part of the Hamiltonian, γ , does not exceed a certain critical value, γ_{\max} , at which the \mathcal{PT} symmetry gets broken. Such linear systems were recently implemented experimentally in optics, due to the fact the paraxial propagation equation for electromagnetic waves can emulate the quantum-mechanical Schrödinger equation. In particular, the \mathcal{PT} -symmetric quantum system may be emulated by waveguides with spatially separated mutually balanced gain and loss elements. Additional interest to the optical realizations of the \mathcal{PT} symmetry has been drawn by the possibility to implement this setting in nonlinear waveguides. Unlike the ordinary models of nonlinear dissipative systems, where stable modes exist as isolated attractors, in \mathcal{PT} -symmetric systems they emerge in continuous families, similar to what is commonly known about conservative nonlinear systems. However, the increase of the gain-loss coefficient, γ , leads to the shrinkage of existence and stability regions for the \mathcal{PT} -symmetric modes, which completely vanish at some $\gamma = \gamma_{\max}$. Especially convenient for the study of such solutions are models of *dual-core couplers*, with the balanced gain and loss applied to different cores, and the cubic nonlinearity acting in both. The objective of the present work is to extend the well-known concepts of quasi-energy and parametric resonances (PRs) to \mathcal{PT} -symmetric systems. In terms of the coupler model, the parametric drive (with ac amplitude V_1 and dc amplitude V_0) can be implemented by making the thickness of the gap between the two cores a periodic function of the evolution variable (propagation distance, in terms of optics), with frequency ω . Using a combination of analytical and numerical methods, we produce the full dynamical chart for both linear and nonlinear versions of the system in the plane of (V_1, V_0) for different values of ω . The charts feature tongues of parametric instability, whose shape has some significant differences from that predicted by the classical theory of the PR in conservative systems.

I. INTRODUCTION AND THE MODEL

A commonly known principle of quantum mechanics is that operators representing physical variables, including the Hamiltonian, must be Hermitian, to guarantee the reality of the respective spectra. Only recently it was found

that the class of physically acceptable Hamiltonians may be extended by admitting operators with anti-Hermitian [dissipative and antidissipative (gain)] parts, if they commute with the \mathcal{PT} (parity-time) transformation [1]. The spectrum of such a \mathcal{PT} -invariant Schrödinger Hamiltonian may be purely real, provided that the strength of the anti-Hermitian part, γ , does not exceeds a critical value, γ_{cr} , at which complex eigenvalues emerge. In the simplest form, a \mathcal{PT} -invariant Hamiltonian contains a complex potential in which the real part is an even function of coordinates, while the imaginary part is odd.

While in the quantum theory this concept remains a rather abstract one, the similarity of the quantum-mechanical Schrödinger equation to the paraxial propagation equation in optics has suggested a possibility to emulate the \mathcal{PT} -symmetry in optical waveguides with symmetrically placed mutually balanced gain and loss elements. This implementation was proposed theoretically [2] and then demonstrated in experiment [3]. Very recently, another experimental realization of the \mathcal{PT} symmetry was reported in a system of coupled electronic oscillators [4].

These possibilities have drawn a great deal of interest to the analysis of various \mathcal{PT} -symmetric dynamical models [5, 6]. In particular, the natural occurrence of the self-focusing in optical media stimulate the study of nonlinear effects in such systems. The interplay of the paraxial diffraction, Kerr nonlinearity, and a spatially periodic complex potential, which represents the \mathcal{PT} -symmetric part of the system, gives rise to bright solitons [7], whose stability was rigorously analyzed in Ref. [8]. Dark solitons have been predicted too in this context, assuming the self-defocusing Kerr nonlinearity [9]. In addition, bright solitons have been predicted in \mathcal{PT} -symmetric systems with the quadratic (second-harmonic-generating) nonlinearity [10]. Systems of another type, which readily maintain \mathcal{PT} -symmetric solitons, and actually make it possible to obtain such solutions and their stability conditions in an exact analytical form, are provided by models of linearly-coupled dual-core waveguides, with the balanced gain and loss applied to the two cores, and the intrinsic Kerr nonlinearity present in each one [11]-[13].

Further, nonlinear modes were studied in many discrete \mathcal{PT} -symmetric systems with the cubic nonlinearity. These include linear [14] and circular [15] chains of coupled \mathcal{PT} elements and aggregates of coupled \mathcal{PT} -symmetric oligomers (dimers, quadrimers, etc.) [16]. General existence, stability and dynamical details of single-component nonlinear \mathcal{PT} -symmetric lattices have been recently discussed in [17].

The inclusion of the Kerr nonlinearity into the conservative part of the system suggests that its gain-and-loss part can be made nonlinear too, by adopting mutually balanced cubic gain and loss terms [18–20]. Effects of combined linear and nonlinear \mathcal{PT} terms on the existence and stability of solitons were studied too [21].

In the usual nonlinear dissipative systems, stable dynamical regimes exist as isolated solutions (*attractors*), such as limit cycles or strange attractors [22] in discrete settings, or dissipative solitons in dissipative media [23]. On the contrary to that, in \mathcal{PT} -symmetric systems stable modes form continuous families, similar to the generic situation in conservative systems. However, the increase of the gain-loss coefficient (γ) in the \mathcal{PT} -symmetric system leads to shrinkage of existence and stability domains for the families, which eventually vanish at $\gamma = \gamma_{\text{cr}}$.

In many cases, quantum systems are driven by time-periodic (ac) external forces. In that case, the eigenstates are characterized by particular values of the quasi-energy, defined as per the Floquet theorem, see, e.g., Ref. [24]. A related concept is the parametric resonance (PR) in linear and nonlinear systems subject to the action of the parametric drive [25]. In the context of \mathcal{PT} -symmetric systems, it is interesting to analyze the realization of the quasi-energy and PRs in ac-driven systems, both linear and nonlinear ones, including mutually balanced gain and loss terms. This analysis is the subject of the present work. We perform it in the framework of a basic model with two degrees of freedom, represented by complex amplitudes ψ_A and ψ_B , and the coupling containing an ac-modulated term, which represents the parametric drive:

$$\begin{aligned} i\frac{d}{dt}\psi_A &= i\psi_A + [V_0 + 2V_1 \cos(\omega t)]\psi_B + \chi|\psi_A|^2\psi_A, \\ i\frac{d}{dt}\psi_B &= -i\psi_B + [V_0 + 2V_1 \cos(\omega t)]\psi_A + \chi|\psi_B|^2\psi_B. \end{aligned} \quad (1)$$

Here the equal gain and loss coefficients in the equations for ψ_A and ψ_B are scaled to be $\gamma \equiv 1$, V_0 and V_1 are strengths of the constant (dc) and ac-modulated couplings, ω is the modulation frequency, and χ is the nonlinearity coefficient, which is taken as $\chi = 0$ or $\chi \equiv 1$ in the linear and nonlinear versions of the system (note that by conjugating (1) and replacing $\psi_A, \psi_B \rightarrow -\psi_A^*, \psi_B^*$ the equations for $\chi = \pm 1$ are transformed into each other, therefore we do not consider $\chi < 0$).

According to the concept of the quasi-energy, quasi-stationary solutions to Eqs. (1) should be sought for as

$$\psi_A(t) = \exp(-iEt) \Psi_A(t), \quad \psi_B(t) = \exp(-iEt) \Psi_B(t), \quad (2)$$

where functions $\Psi_{A,B}(t)$ are periodic functions with period $2\pi/\omega$, and the quasi-energy E belongs to interval $0 < E < 2\pi/\omega$. A corollary of Eqs. (1) is the balance equation for the total power in the presence of the mutually symmetric

gain and loss [17]

$$\frac{d}{dt} (|\psi_A|^2 + |\psi_B|^2) = 2 (|\psi_A|^2 - |\psi_B|^2). \quad (3)$$

This system can be implemented as a model of a dual-core waveguide operating in the CW (continuous-wave) regime, so that Eqs. (1) do not include terms accounting for the transverse diffraction or group-velocity dispersion, in the spatial-domain and temporal-domain realizations, respectively. Variable t is actually the propagation distance, and the ac modulation represents periodic variation of the thickness of the gap separating the cores [26]. As suggested in Refs. [11], terms $\pm i\psi_{A,B}$ in Eqs. (1) represent the gain and loss applied to the two cores. A similar system, without the ac-modulating terms, but with the addition of cubic gain and loss terms, was proposed as a model of a \mathcal{PT} -symmetric dimer in Ref. [19].

The main issue considered in this work is the effect of the \mathcal{PT} symmetry on PRs in the framework of the linear and nonlinear versions of system (1). First, in Section II we develop an analytical approach, predicting at what values of V_0 the ac drive with fixed ω gives rise to PR at infinitesimally small V_1 , and how tongues of the parametric instability expand with the increase of V_1 . Comprehensive dynamical charts of the linearized version of system (1) and the full nonlinear system, built on the basis of systematic numerical simulations, are presented in Sections III and IV, respectively. The structure of the charts at large V_1 is very different from the picture of PRs in usual (non- \mathcal{PT}) driven dynamical systems. The paper is concluded by Section V.

II. THE ANALYTICAL APPROACH

A. The perturbative analysis of the linear system

With a small amplitude of the ac drive, V_1 , a perturbative solution to the linearized version of Eqs. (1), with spatial quasi-frequency E (or quasi-energy, in terms of quantum \mathcal{PT} -symmetric systems), is looked for in the form of Eq. (2), adopting the lowest-order truncation for the periodic amplitudes [25],

$$\Psi_{A,B}(t) = \Psi_{A,B}^{(0)} + \Psi_{A,B}^{(+)} e^{-i\omega t} + \Psi_{A,B}^{(-)} e^{+i\omega t}, \quad (4)$$

with constants $\Psi_A^{(0,\pm)}, \Psi_B^{(0,\pm)}$. Substituting this ansatz into Eqs. (1) and keeping, in line with the form of truncation (4), the zeroth and first harmonics in the ensuing expansion, gives rise to a system of linear homogeneous equations for the vectorial set of six amplitudes,

$$\Psi = \left\{ \Psi_A^{(0)}, \Psi_A^{(+)}, \Psi_A^{(-)}, \Psi_B^{(0)}, \Psi_B^{(+)}, \Psi_B^{(-)} \right\}. \quad (5)$$

Nontrivial solutions exist under the condition that the determinant of the system vanishes, which leads to the following equation for E :

$$\begin{vmatrix} i-E & 0 & 0 & V_0 & V_1 & V_1 \\ 0 & i-E-\omega & 0 & V_1 & V_0 & 0 \\ 0 & 0 & i-E+\omega & V_1 & 0 & V_0 \\ V_0 & V_1 & V_1 & -i-E & 0 & 0 \\ V_1 & V_0 & 0 & 0 & -i-E-\omega & 0 \\ V_1 & 0 & V_0 & 0 & 0 & -i-E+\omega \end{vmatrix} = 0. \quad (6)$$

Each eigenvalue is associated with a zero eigenvector Ψ of matrix (6). Complex solutions of Eq. (6) for eigenvalues E imply instability of the linear system due to the spontaneous breaking of the \mathcal{PT} symmetry, or excitation of a PR, or an interplay of both mechanisms (as shown below, all these cases are possible). Real eigenvalues E correspond to stable oscillatory solutions.

In the zeroth-order approximation, $V_1 = 0$, Eq. (6) yields an obvious result: the spectrum remains real under the condition

$$V_0^2 > (V_0^2)_{\min} \equiv 1 \quad (7)$$

[more explicitly, $(V_0^2)_{\min} = \gamma^2$, if scaling $\gamma \equiv 1$ for the gain-loss coefficient is not fixed]. In this approximation, the six eigenvalues are

$$E = \pm \sqrt{V_0^2 - 1}, E = \pm \omega \pm \sqrt{V_0^2 - 1}, \quad (8)$$

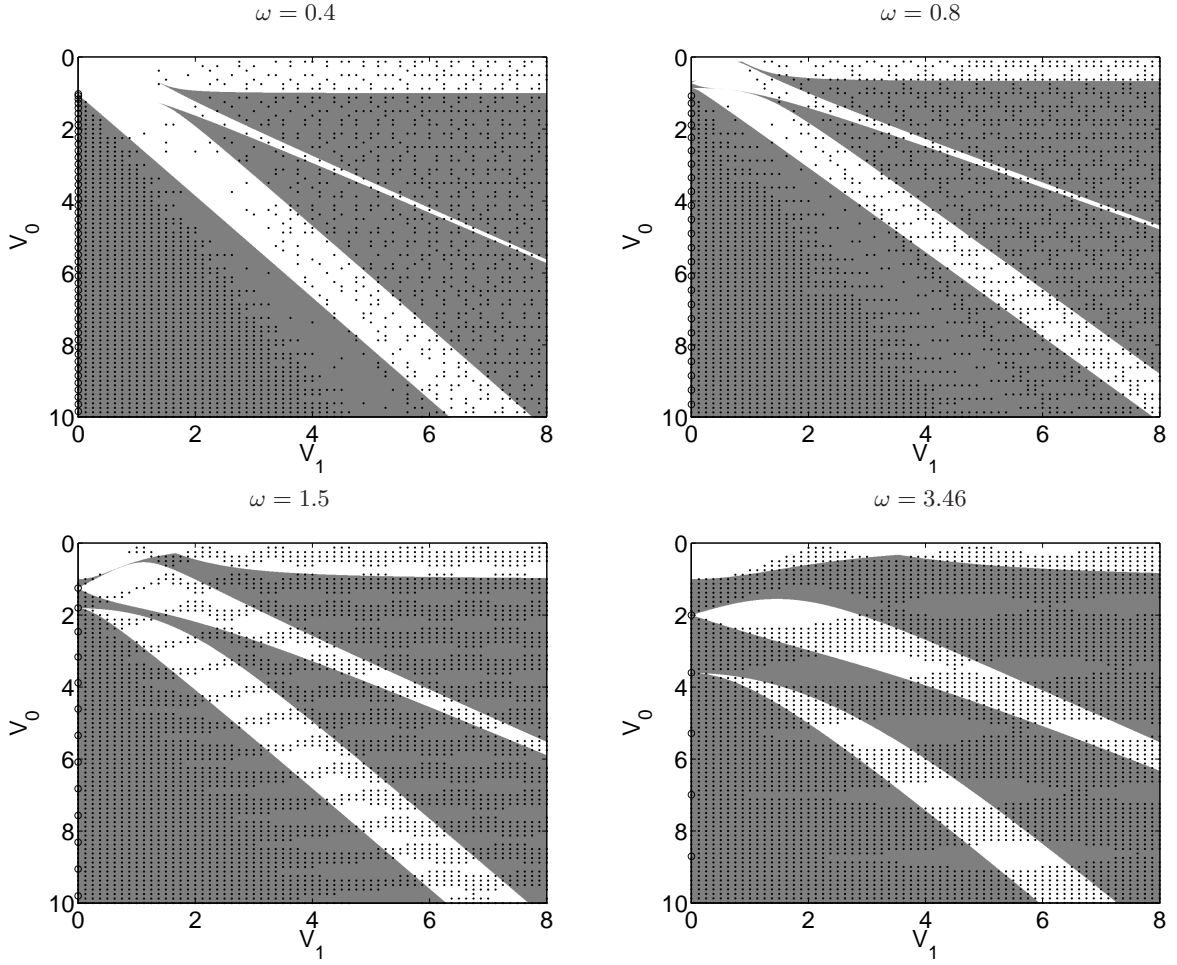


FIG. 1: Dark and white backgrounds represent areas of stability and instability of the linear version of system (1) with $\chi = 0$, as predicted by the numerical solution of perturbative equation (6), in the parameter plane of (V_1, V_0) at several fixed values of ω (the equation produces solely real eigenvalues E in the stable areas). The plots are superimposed with thin dots denoting parameter values for which direct simulations of the linear version of Eqs. (1) demonstrate stability, unstable solutions populating areas in the parameter plane which are not covered by dots. The dotted grid was built with steps $\Delta V_1 = \Delta V_0 = 0.125$. The circles on the left vertical axis, corresponding to $V_1 \rightarrow 0$, correspond to discrete points at which the parametric resonances are predicted by Eq. (10).

where different \pm signs are mutually independent.

The prediction for the stability and instability areas in the plane of the ac and dc coupling strengths, (V_1, V_0) , at four different several values of the driving frequency,

$$\omega = 0.4, 0.8, 1.5, 2\sqrt{3} \approx 3.46, \quad (9)$$

as predicted by a numerical solution of the algebraic equation (6), is displayed in Fig. 1. The plots also show stability areas (covered by dots) as obtained in Section III by means of systematic direct simulations of the linear version of Eqs. (1), i.e. the one with $\chi = 0$, as well as circles on the vertical axis corresponding to parametric resonances as described in the next subsection.

B. Parametric resonances

In the limit of $V_1 \rightarrow 0$, when the eigenfrequency of free oscillations in the linearized system is $E = \sqrt{V_0^2 - 1}$, see Eq. (8), the standard theory [25] produces the PR (i.e., the onset of the instability of the linear system, different from

the instability due to breaking of the \mathcal{PT} symmetry) at the following values of the driving frequency:

$$\omega_{\text{res}}^{(n)} = \frac{2}{n} \sqrt{V_0^2 - 1}, \quad (10)$$

where $n = 1, 2, 3, \dots$ is the order of the resonance. Thus, for given driving frequency ω , Eq. (10) predicts the resonance at

$$(V_0)_{\text{res}}^{(n)} = \sqrt{1 + (n\omega/2)^2}. \quad (11)$$

In Fig. 1, circles on the vertical axis in each plot mark positions of the PR as predicted by Eq. (11).

Note that in the case of $\omega = 0.4$, Eq. (11) yields values

$$(V_0)_{\text{res}}^{(1)} = \sqrt{1.04} \approx 1.02, \quad (V_0)_{\text{res}}^{(2)} = \sqrt{1.16} \approx 1.08, \quad (12)$$

which are close to the above-mentioned critical value, $(V_0)_{\text{min}} = 1$, induced by the balanced combination of the gain and loss terms, see Eq. (7). The wide and narrow instability stripes, observed in the panel of Fig. 1 corresponding to $\omega = 0.4$, originate from two critical values (12) at small values of V_1 . This situation actually implies a *merger* of the \mathcal{PT} -breaking and PR-induced instabilities for relatively small values of ω .

At larger ω , the \mathcal{PT} and PR instabilities are clearly separated at $V_1 \rightarrow 0$. For instance, at $\omega = 2\sqrt{3} \approx 3.46$, Eq. (11) yields $(V_0)_{\text{res}}^{(1)} = 2$ for the fundamental parametric resonance ($n = 1$). In accordance with this, the respective panel of Fig. 1 features a separate instability tongue, originating, at small V_1 , from point $V_0 = 2$, and expanding with the increase of V_1 . The additional tongue observed in the same panel, originating from $V_0 = \sqrt{13} \approx 3.6$ at $V_1 = 0$, is predicted by Eq. (11) with $n = 2$. These tongues are quite similar to those known in the usual (non- \mathcal{PT}) model of the parametric instability.

III. DIRECT SIMULATIONS OF THE LINEAR SYSTEM ON THE PARAMETER GRID

To produce an accurate stability chart for the linear version of the underlying system, i.e., Eqs. (1) with $\chi = 0$, we have carried out systematic simulations of the equations on a square grid in the plane of (V_1, V_0) with limits $0 \leq V_1 \leq 8$, $0 \leq V_0 \leq 10$ and steps $\Delta V_1 = \Delta V_0 = 0.125$. This has been done at four fixed values of the driving frequency from set (9). Initial values $\{\psi_A(0), \psi_B(0)\}$ for each run of the simulations were calculated as per Eqs. (2) and (4), with set (5) calculated as a zero eigenvector of matrix (6). The simulations were performed by means of a standard 4th order Runge-Kutta code. To check the accuracy of the calculations, we verified that the numerical solutions would satisfy balance equation (3).

To distinguish stable and unstable solutions, we checked whether the maximum of $|\psi_A(t)|$ or $|\psi_B(t)|$ would double after a sufficiently long period of time, in comparison to the modulation period, $2\pi/\omega$. It has been found that the lack of the doubling is an appropriate indicator of the stability of a given solution (in other words, the solutions which could be identified as stable ones would never double their largest site modulus). Each parameter set categorized as stable is marked by a dot in Fig. 1. Unstable solutions were identified as those breaking the above-mentioned no-doubling condition, which was followed by visual checks. In Fig. 1, unstable solutions are represented by missing dots on the selected grid.

Figure 1 clearly demonstrates interesting connections but also nontrivial differences between the present stability charts and those well known in the PR theory. Indeed, different numerical stability tongues originating from $V_1 \rightarrow 0$ do not bend down, as in the usual theory, but keep the direction parallel to the axis of V_1 . This difference suggests that the truncation adopted in Eq. (4) becomes rather irrelevant at large V_1 , and a larger number of harmonics get involved into the dynamics, as corroborated by spectra of particular solutions displayed below. With the decrease of ω , the number of tongues becomes large, while their widths and gaps between adjacent ones get small. At small ω , the stability chart features a complex small-scale structure, which has no counterpart in the ordinary PR theory. It is important to point out that while the quasi-energy based theory of Section II.A is expected (and found in Fig. 1) to be valid for small V_1 , the PR theory of section II.B is especially relevant in a different limit. In particular, it appears to accurately capture the dynamics in the case of large ω where the PR points are no longer clustered and their tongues accordingly shrunk. It can be clearly discerned in the Figure that the horizontal tongues for the cases of e.g. $\omega = 1.2$ and 1.6 appear to naturally emanate from the PR points of $V_1 \rightarrow 0$. An additional interesting point to mention in that light is that higher order resonances appear to be initiated “deeper” along the V_1 axis, although this may also be a consequence of the finite horizon of our simulations (and of the weak growth rate of these instabilities for small V_1).

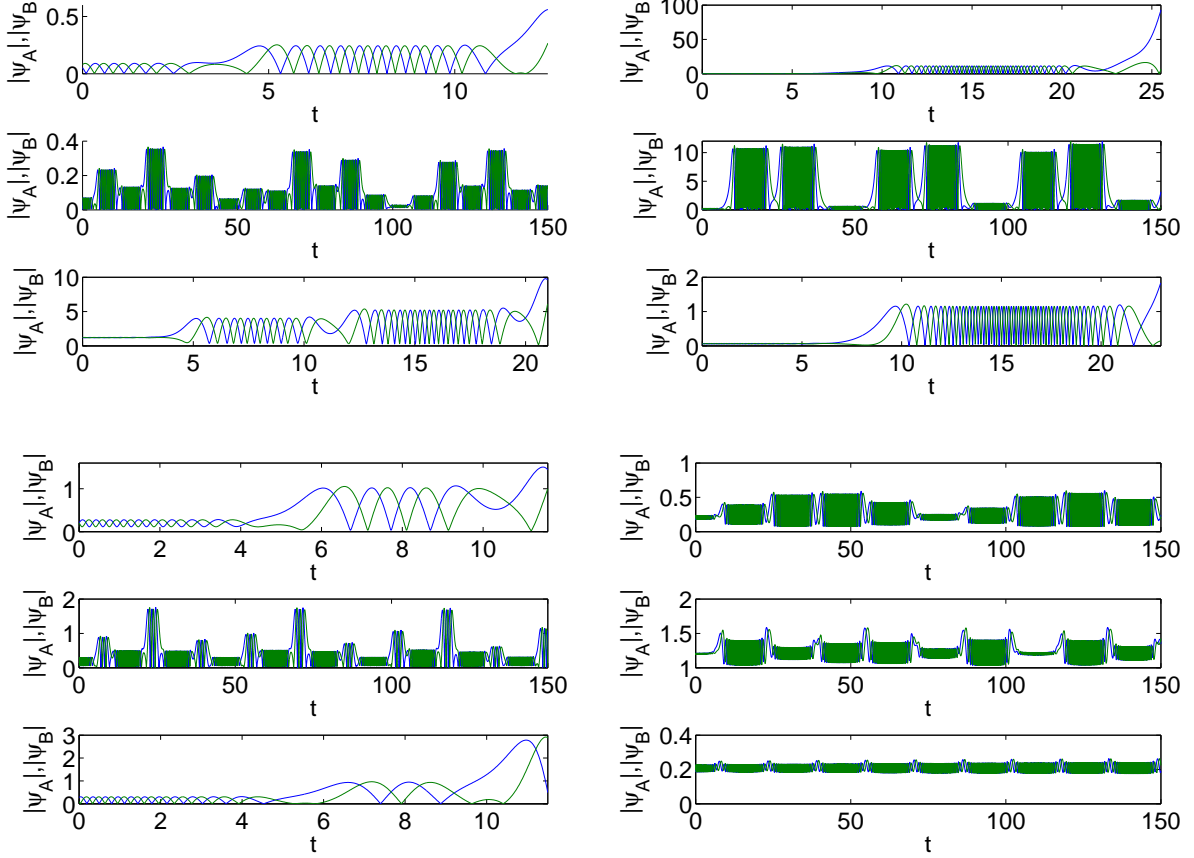


FIG. 2: Plots of solutions $|\psi_A(t)|, |\psi_B(t)|$ produced by the numerical simulations of the linear version of Eqs. (1) for parameter values corresponding to a vertical cut in Fig. 1 at $V_1 = 3.25$. These plots confirm that actually present black dots and missing ones (empty sites of the grid) in Fig. 1 represent stable and unstable solutions, respectively. Values of V_0 corresponding to the left and right columns (from top to bottom) are 0, 0.5, 1, 3, 3.5, 4, and 5.5, 6, 6.5, 7.5, 8, 8.5, respectively.

Figure 2 shows characteristic examples of the solutions for select combinations of parameter values, both stable (quasi-periodic) and unstable (growing) ones. Due to the presence of the gain in the system, unstable solutions proceed to grow indefinitely (according to an -at most- exponential rate [17]). As a result, at some point in time, after the temporal interval displayed in respective panels of Fig. 2, each amplitude increases rapidly (eventually the evolution also accrues numerical error).

For a few stable oscillatory solutions, Fig. 3 shows the power spectra generated by means of the DFFT (discrete fast Fourier transform),

$$\text{power}_{A,B}(f_k) = \left| \frac{1}{N} \sum_{j=1}^N \psi_{A,B}(t_j) \exp \left(2\pi i \frac{(j-1)k}{N} \right) \right|^2, \quad (13)$$

where $t_j = j\Delta t$, t_N is the total integration time and $f_k \in \frac{1}{\Delta t N} \{1, \dots, N/2\}$ for N even. All the spectra show a prominent peak at the driving frequency $\omega/(2\pi)$. One also observes a set of weaker higher-frequency peaks corresponding to the frequency multiplication by the parametric drive.

To resolve the higher frequencies (smaller periods), we have performed FFT on smaller windows. For example, within the first few seconds of the simulations for small ω we observe a dominant frequency in the spectrum consistent with the prediction, $f = \sqrt{(V_0 + 2V_1)^2 - 1}/(2\pi)$, given by Eq. (8) with $\omega = 0$. As $\psi_A(t)$ and $\psi_B(t)$ evolve in time, the high frequencies lead to modulations. For parameter values (V_0, V_1) which are buried deepest in stability regions in Fig. 1, the solutions feature the least amount of such fluctuations at high frequencies. These fluctuations account for the small-amplitude pattern in the high-frequency part of the spectra in Fig. 3, which appears when the FFT is

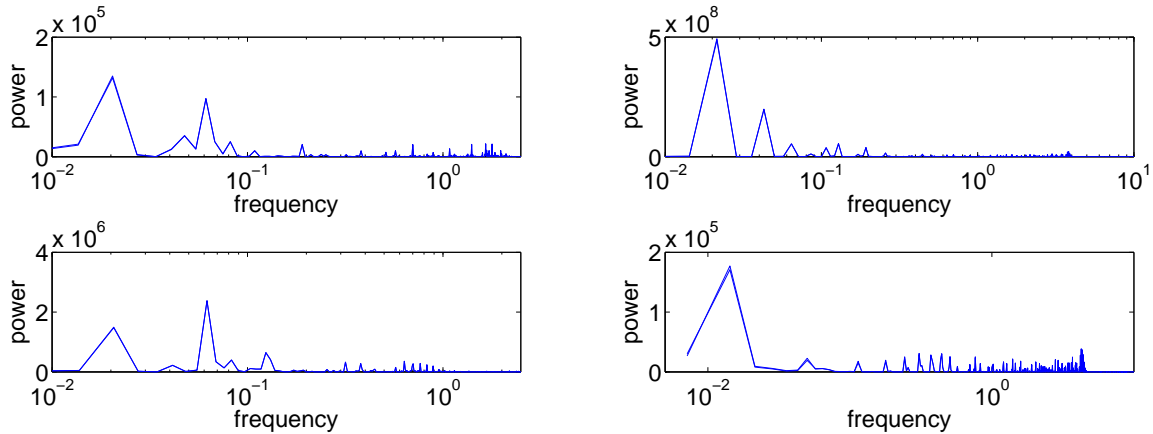


FIG. 3: For $\omega = 0.4$, plotted on the logarithmic scale of the frequency are power spectra computed as per Eq. (13) for the following values of the parameters: $(V_1, V_0) = (3.25, 0.5)$ in the top left, $(3.25, 3.5)$ in the bottom left, $(3.25, 6)$ in the top right and $(3.25, 7.5)$ in the bottom right. The frequency in the plots is f defined as in Eq. (13), and the power spectra for both components of stable solutions completely overlap. The corresponding solutions $\psi_{A,B}(t)$ are displayed in Fig. 2. A prominent peak is found at frequency $0.0637 = (\omega = 0.4)/2\pi$.

performed on a large interval, such as $[0, 250]$. All of the frequencies which appear in Fig. 3 are linear combinations of the $\omega = 0$ prediction and the driving frequency $\omega/(2\pi)$.

IV. THE NONLINEAR PROPAGATION

As indicated above, the initial values of (ψ_A, ψ_B) , used in the simulations of the linear version of Eqs. (1), were generated as per Eqs. (2) and (4), into which zero eigenvectors (5) of the matrix from Eq. (6) were substituted. We now use the same inputs for the systematic simulations of the full nonlinear form of Eqs. (1) with $\chi = 1$.

Figure 4 shows the so-generated nonlinear counterpart of Fig. 1, on the same grid of parameter values. In the upper two predicted-as-stable (gray) regions of Fig. 4, the tests generally show that the solutions are more likely to be unstable, in comparison with the linear system. In the inner portions of the lower gray regions, many solutions stay stable in the presence of the nonlinearity, while they are more likely to be unstable at the boundary of the region, in comparison with the linear case.

Some stable solutions of the linear system remain apparently robust when the nonlinearity is added, but with different amplitudes, in comparison to their linear counterparts. Profiles shown in Figs. 5 and 6 are nonlinear extensions of those displayed above in Fig. 2. As in the case of the linear system, the balance equation (3) remains valid for stable solutions, while the unstable solutions grow indefinitely with the (typically) exponential growth rate predicted in [17].

Finally, it is relevant to emphasize that the addition of the nonlinearity does not necessarily lead to a partial destabilization of the solutions, as the effect may be the opposite. In particular, there are a few dots in Fig. 4 that do not appear in Fig. 1. Profiles of a few solutions in the linear and nonlinear systems, corresponding to three of these dots, are displayed in Fig. 7.

V. CONCLUSIONS

We have introduced, arguably, the simplest model which opens the way to studying the concept of quasi-energy and PRs (parametric resonances), with ensuing instability, in \mathcal{PT} -symmetric systems, incorporating spatially separated and mutually balanced gain and loss elements. The parametric drive is introduced in the form of the periodic (ac) modulation of the coefficient of the coupling between the two degrees of freedom. The onset and development of the parametric instability at a small amplitude of the ac drive is predicted analytically. The full picture is obtained by means of systematic simulations of both linear and nonlinear versions of the system. At large values of the driving frequency, ω , the tongues of the parametric instability originate, with the increase of the driving amplitude (V_1), at values of the coupling constant (V_0) predicted by the analytical consideration of the resonance points. However,

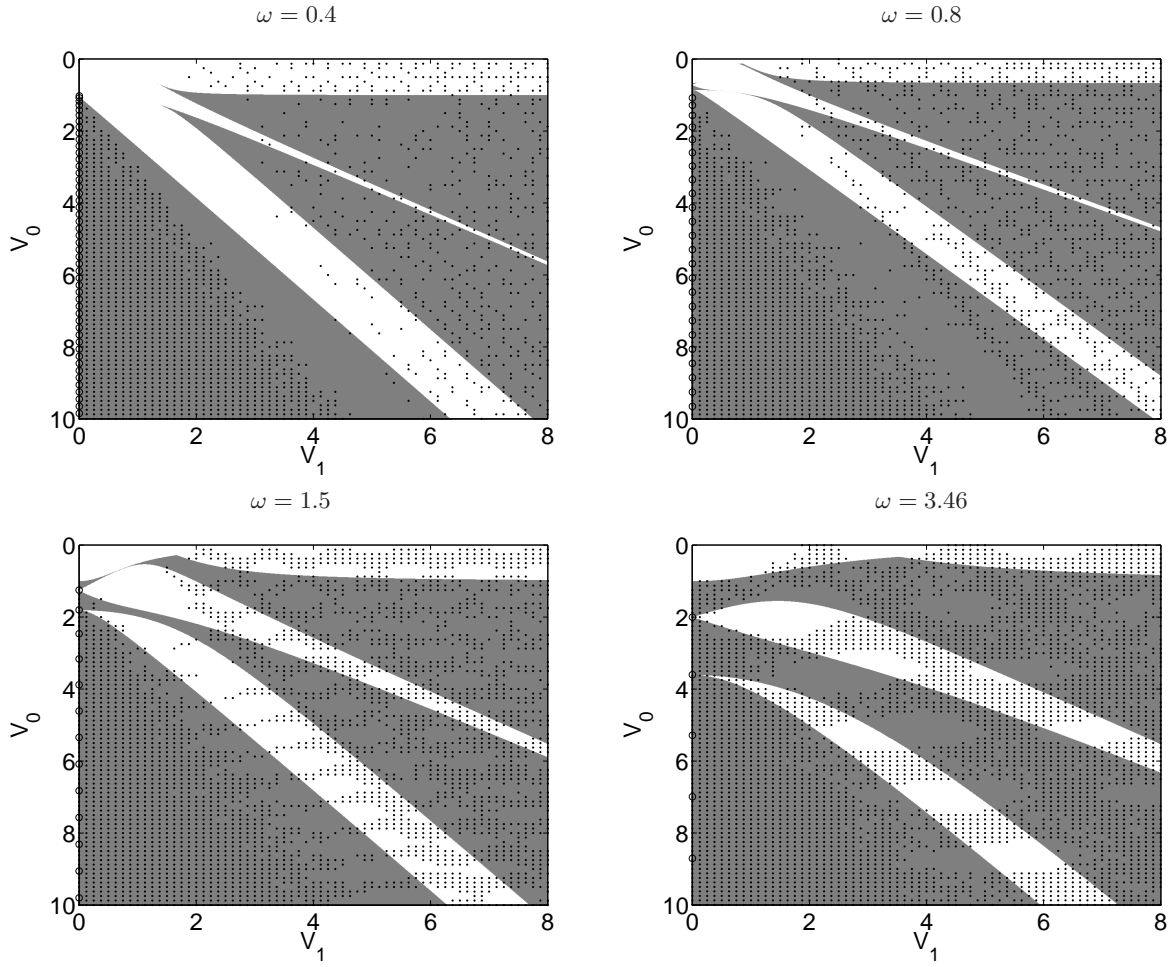


FIG. 4: The same as in Fig. 1, but with dots representing robust numerical solutions of the full nonlinear equations (1). See Figs. 5 and 6 for profiles of typical solutions.

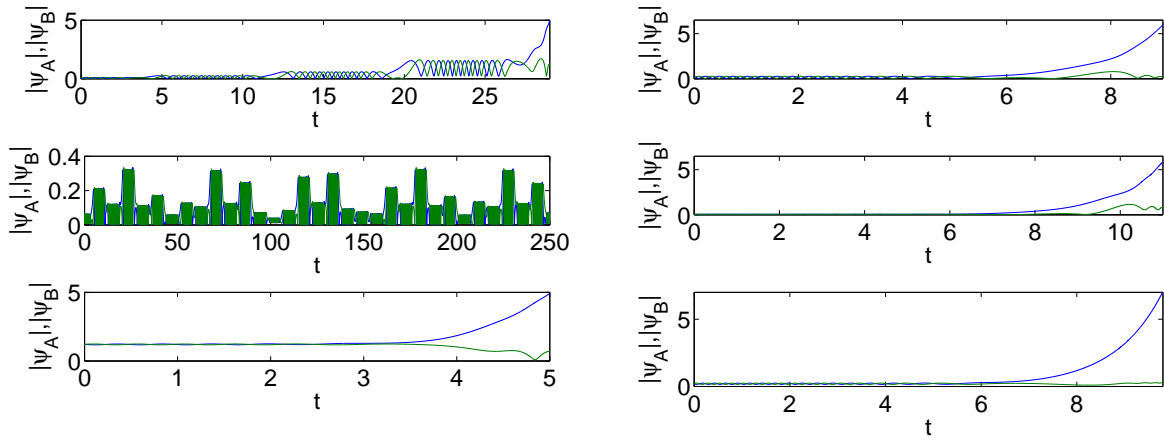


FIG. 5: Each plot shows solutions evolving according to nonlinear equations (1). Parameter values (V_1, V_0) follow the same pattern as the top six plots in Fig. 2: $(3.25, 0), (3.25, 0.5), (3.25, 1)$ on the left and $(3.25, 5.5), (3.25, 6), (3.25, 6.5)$ on the right. The respective initial amplitudes of each solution are: $(|\psi_A|, |\psi_B|) = (0.0530, 0.0868), (0.0225, 0.0712), (1.2052, 1.2052), (0.2516, 0.1538), (0.2087, 0.2087), (0.0607, 0.0607)$. Of the two stable solutions of the linear system, only one remains stable in the nonlinear case.

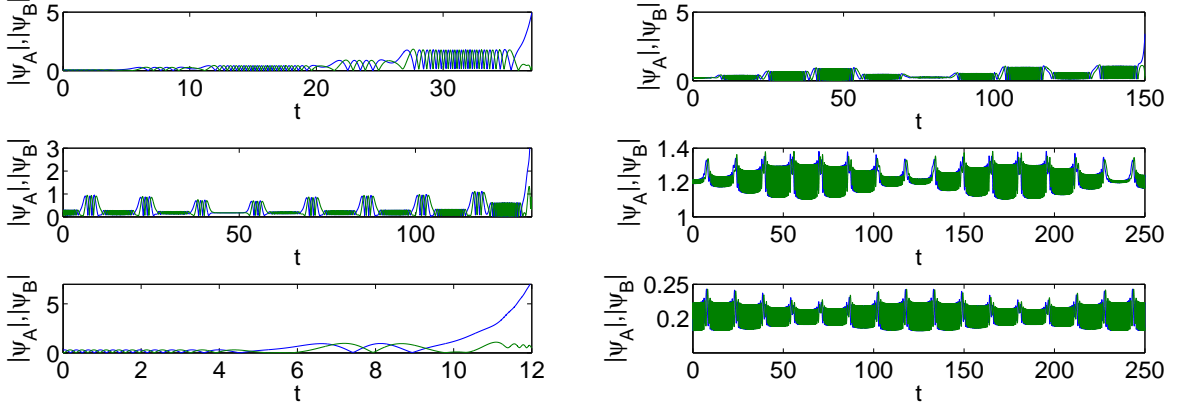


FIG. 6: The same as in Fig. 5. Values (V_1, V_0) follow the same pattern as the bottom six plots of Figure 2: $(3.25, 3), (3.25, 3.5), (3.25, 4), (3.25, 7.5), (3.25, 8), (3.25, 8.5)$. Respective initial amplitudes of the wave functions are $(|\psi_A|, |\psi_B|) = (0.2095, 0.2095), (0.2098, 0.2098), (0.2098, 0.2098), (0.2089, 0.2089), (0.2089, 0.2089), (1.2052, 1.2052)$. Of the four stable solutions of the corresponding linear system, two become unstable, and two remain stable, with amplitudes differing from their counterparts in the linear system.

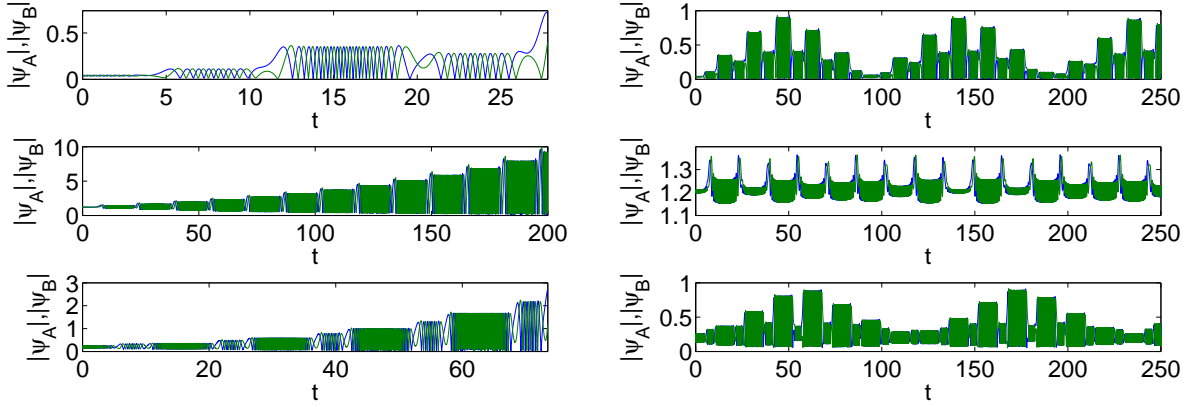


FIG. 7: Plots of $|\psi_A(t)|, |\psi_B(t)|$ are shown at parameter values which correspond to missing dots in Fig. 1 (unstable in the linear system) and dots in Fig. 4 (stable in the nonlinear system). The left and right columns correspond, respectively, to the linear and nonlinear propagation. Values (V_1, V_0) from top to bottom are $(3.5, 1.5), (4, 9.5), (7, 8)$. For the nonlinear simulations, initial values are $(|\psi_A|, |\psi_B|) = (0.0437, 0.0437), (1.2059, 1.2059), (0.2076, 0.2076)$.

the continuation of the PR tongues with the increase of V_1 in the \mathcal{PT} -symmetric system follows a scenario which is very different from the usual parametrically driven system: instead of bending down to larger values of V_0 , the tongues continue in directions parallel to the V_1 axis. The decrease of ω makes the system of parallel tongues denser, eventually replacing the relatively simple system of parallel instability tongues by a complex small-scale structure. While the parametric resonance picture is an accurate predictor of the tongue formation at large ω , the quasi-energy method yields reasonably accurate results at small V_1 . The inclusion of the nonlinearity gradually deforms the picture, destabilizing a part of originally stable dynamical regimes, and stabilizing a few originally unstable ones. In principle, however, as may be expected the main effect of the nonlinearity is in enhancing the region of instability.

This analysis may be extended in various ways, adding more terms to the system. In particular, a straightforward generalization may include nonlinear gain and loss terms, in addition to the linear pair of such terms, cf. Refs. [18–20]. Extensions beyond the dimer case to oligomers and eventually to lattices would also be particularly interesting to consider [14–17]. Relevant themes are currently under consideration and will be presented in future publications.

Acknowledgment

This work was supported, in a part, by the Binational (US-Israel) Science Foundation through grant No. 2010239.

-
- [1] C. M. Bender, Rep. Prog. Phys. **70**, 947 (2007).
 - [2] A. Ruschhaupt, F. Delgado, and J. G. Muga, J. Phys. A: Math. Gen. **38**, L171 (2005).
 - [3] A. Guo, G. J. Salamo, D. Duchesne, R. Morandotti, M. Volatier-Ravat, V. Aimez, G. A. Siviloglou, and D. N. Christodoulides, Phys. Rev. Lett. **103**, 093902 (2009); C. E. Rüter, K. G. Makris, R. El-Ganainy, D. N. Christodoulides, M. Segev, and D. Kip, Nature Phys. **6**, 192 (2010).
 - [4] N. Bender, S. Factor, J. D. Bodyfelt, H. Ramezani, D. N. Christodoulides, F. M. Ellis, and T. Kottos, Phys. Rev. Lett. **110**, 234101 (2013); see also J. Schindler, A. Li, M.C. Zheng, F.M. Ellis and T. Kottos, Phys. Rev. A **84**, 040101 (2011).
 - [5] See special issues: H. Geyer, D. Heiss, and M. Znojil, Eds., J. Phys. A: Math. Gen. **39**, *Special Issue Dedicated to the Physics of Non-Hermitian Operators (PHHQP IV)* (University of Stellenbosch, South Africa, 2005) (2006); A. Fring, H. Jones, and M. Znojil, Eds., J. Math. Phys. A: Math Theor. **41**, *Papers Dedicated to the Subject of the 6th International Workshop on Pseudo-Hermitian Hamiltonians in Quantum Physics (PHHQPVI)* (City University London, UK, 2007) (2008); C. Bender, A. Fring, U. Günther, and H. Jones, Eds., *Special Issue: Quantum Physics with non-Hermitian Operators*, J. Math. Phys. A: Math Theor. **41**, No. 44 (2012).
 - [6] K. G. Makris, R. El-Ganainy, D. N. Christodoulides, and Z. H. Musslimani, Int. J. Theor. Phys. **50**, 1019 (2011).
 - [7] Z. H. Musslimani, K. G. Makris, R. El-Ganainy, and D. N. Christodoulides, Phys. Rev. Lett. **100**, 030402 (2008); Z. Lin, H. Ramezani, T. Eichelkraut, T. Kottos, H. Cao, and D. N. Christodoulides, Phys. Rev. Lett. **106**, 213901 (2011); X. Zhu, H. Wang, L.-X. Zheng, H. Li, and Y.-J. He, Opt. Lett. **36**, 2680 (2011); C. Li, H. Liu, and L. Dong, Opt. Exp. **20**, 16823 (2012); C. M. Huang, C. Y. Li, and L. W. Dong, *ibid.* **21**, 3917 (2013).
 - [8] S. Nixon, L. Ge, and J. Yang, Phys. Rev. A **85**, 023822 (2012).
 - [9] H. G. Li, Z. W. Shi, X. J. Jiang, and X. Zhu, Opt. Lett. **36**, 3290 (2011); V. Achilleos, P. G. Kevrekidis, D. J. Frantzeskakis, and R. Carretero-González, Phys. Rev. A **86**, 013808 (2012); see also V. Achilleos, P.G. Kevrekidis, D.J. Frantzeskakis, R. Carretero-González, arXiv:1202.1310.
 - [10] F. C. Moreira, F. K. Abdullaev, V. V. Konotop, and A. V. Yulin, Phys. Rev. A **86**, 053815 (2012); F. C. Moreira, V. V. Konotop, and B. A. Malomed, *ibid.* **87**, 013832 (2013).
 - [11] R. Driben and B. A. Malomed, Opt. Lett. **36**, 4323 (2011); N. V. Alexeeva, I. V. Barashenkov, A. A. Sukhorukov, and Y. S. Kivshar, Phys. Rev. A **85**, 063837 (2012); I. V. Barashenkov, S. V. Suchkov, A. A. Sukhorukov, S. V. Dmitriev, and Y. S. Kivshar, *ibid.* **86**, 053809 (2012).
 - [12] F. K. Abdullaev, V. V. Konotop, M. Ögren, and M. P. Sørensen, Opt. Lett. **36**, 4566 (2011); R. Driben and B. A. Malomed, EPL **96**, 51001 (2011); *ibid.* **99**, 54001 (2012).
 - [13] Yu. V. Bludov, V. V. Konotop, and B. A. Malomed, Phys. Rev. A **87**, 013816 (2013).
 - [14] S. V. Dmitriev, A. A. Sukhorukov, and Y. S. Kivshar, Opt. Lett. **35**, 2976 (2010); S. V. Suchkov, B. A. Malomed, S. V. Dmitriev, and Y. S. Kivshar, Phys. Rev. E **84**, 046609 (2011); S. V. Suchkov, A. A. Sukhorukov, S. V. Dmitriev, and Y. S. Kivshar, EPL **100**, 54003 (2012); D. A. Zezyulin and V. V. Konotop, Phys. Rev. Lett. **108**, 213906 (2012).
 - [15] D. Leykam, V. V. Konotop, and A. S. Desyatnikov, Opt. Lett. **38**, 371 (2013); I. V. Barashenkov, L. Baker, and N. V. Alexeeva, Phys. Rev. A **87**, 033819 (2013).
 - [16] K. Li and P. G. Kevrekidis, Phys. Rev. E **83**, 066608 (2011); V. V. Konotop, D. E. Pelinovsky, and D. A. Zezyulin, EPL **100**, 56006 (2012); J. D'Ambroise, P. G. Kevrekidis, and S. Lepri, J. Phys. A: Math. Theor. **45**, 444012 (2012); K. Li, P. G. Kevrekidis, B. A. Malomed, and U. Günther, *ibid.* **45**, 444021 (2012); M. Kreibich, J. Main, H. Cartarius, and G. Wunner, Phys. Rev. A **87**, 051601(R) (2013).
 - [17] P.G. Kevrekidis, D.E. Pelinovsky, D.Y. Tyugin, SIAM J. Appl. Dyn. Syst. **12** 1210-36 (2013); see also arXiv:1307.2973 and J. Pickton, H. Susanto, arXiv:1307.2788.
 - [18] F. Kh. Abdullaev, Y. V. Kartashov, V. V. Konotop, and D. A. Zezyulin, Phys. Rev. A **83**, 041805(R) (2011); D. A. Zezyulin, Y. V. Kartashov, V. V. Konotop, Europhys. Lett. **96**, 64003 (2011).
 - [19] A. E. Miroshnichenko, B. A. Malomed, and Y. S. Kivshar, Phys. Rev. A **84**, 012123 (2011).
 - [20] M. Duanmu, K. Li, R.L. Horne, P.G. Kevrekidis and N. Whitaker, Phil. Trans. R. Soc. A **371**, 20120171 (2013).
 - [21] Y. He, X. Zhu, D. Mihalache, J. Liu, and Z. Chen, Phys. Rev. A **85**, 013831 (2012); Opt. Commun. **285**, 3320 (2012).
 - [22] E. Ott, *Chaos in Dynamical Systems* (Cambridge University Press: Cambridge, 1993).
 - [23] B. A. Malomed, Physica D **29**, 155 (1987); S. Fauve, O. Thual, Phys. Rev. Lett. **64**, 282 (1990); W. van Saarloos and P. C. Hohenberg, Phys. Rev. Lett. **64**, 749 (1990); V. Hakim, P. Jakobsen, and Y. Pomeau, Europhys. Lett. **11**, **19** (1990); B. A. Malomed and A. A. Nepomnyashchy, Phys. Rev. A **42**, 6009 (1990); P. Marcq, H. Chaté, and R. Conte, Physica D **73**, 305 (1994); T. Kapitula and B. Sandstede, J. Opt. Soc. Am. B **15**, 2757 (1998); A. Komarov, H. Leblond, and F. Sanchez, Phys. Rev. E **72**, 025604 (2005); J. N. Kutz, SIAM Rev. **48**, 629 (2006).
 - [24] H. P. Breuer and M. Holthaus, Ann. Phys. **211**, 249 (1991).
 - [25] L. D. Landau and E. M. Lifshitz, *Mechanics* (Nauka Publishers: Moscow, 1973).
 - [26] P. L. Chu, B. A. Malomed, G. D. Peng, and I. Skinner, Phys. Rev. E **49**, 5763 (1994).